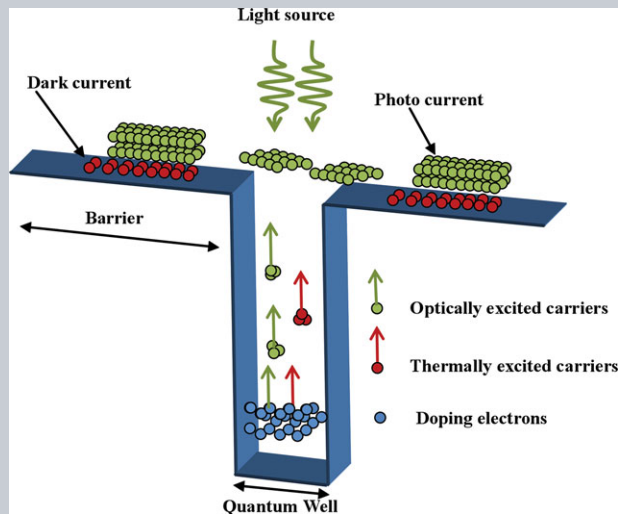


LASER & PHOTONICS REVIEWS

Abstract With the modern development of infrared laser sources such as broadly tunable quantum cascade lasers and frequency combs, applications of infrared laser spectroscopy are expected to become widespread. Consequently, convenient infrared detectors are needed, having properties such as fast response, high efficiency, and room-temperature operation. This work investigated conditions to achieve near-room-temperature photon-noise-limited performance of quantum well infrared photodetectors (QWIPs), in particular the laser power requirement. Both model simulation and experimental verification were carried out. At 300 K, it is shown that the ideal performance can be reached for typical QWIP designs up to a detection wavelength of 10 μm . At 250 K, which is easily reachable with a thermoelectric Peltier cooler, the ideal performance can be reached up to 12 μm . QWIPs are therefore suitable for detection and sensing applications with devices operating up to or near room temperature.



Near-room-temperature photon-noise-limited quantum well infrared photodetector

Ming Rui Hao^{1,*}, Yao Yang¹, Shuai Zhang¹, Wen Zhong Shen^{1,*}, Harald Schneider^{1,2,*}, and Hui Chun Liu¹

1. Introduction

Quantum well infrared photodetectors (QWIPs) [1] have been applied to focal plane arrays (FPAs) for thermal imaging [2, 3] and high-speed and high-frequency detectors in the mid- and long-wavelength infrared spectral ranges [4, 5]. New applications, such as trace-gas sensing based on quantum cascade lasers (QCLs) have drawn wide attention [6, 7].

Infrared photodetectors generally work at low temperatures to minimize the dark current and dark current noise. Some new designs, such as photovoltaic [8] or quantum cascade detectors [9], are investigated to improve the signal-to-noise ratio. For weak signals, it is usually desirable that photodetectors operate under background-limited performance (BLIP) condition. The BLIP temperature of mid-infrared photodetectors is around the liquid nitrogen temperature range, which is also reached by using closed-cycle coolers. One way to optimize the detectors for high-temperature operation is using efficient resonant cavities [10]. However, for some applications (e.g., gas sensing [11–13] and heterodyne detection [14, 15]) involving a strong light source, the photocurrent can be made larger

than the dark current, such that the photodetector would then still have a good signal-to-noise ratio (SNR) at high operating temperatures. State-of-the-art QCLs for 4–14 μm wavelength coverage provide single-mode light emission with high power up to hundreds of milliwatts [16]. Illuminated by such a QCL, the signal photocurrent can be higher than the dark current, as well as the background photocurrent, even for room- or near-room-temperature operation.

In this work, we use the three-dimensional carrier drift model to simulate the dark current of QWIPs at high operating temperatures. The temperature effect on Fermi energy is taken into consideration, which is essential in this high-temperature region. Based on simulation results, we predict the laser power requirement to reach photon-noise-limited performance for QWIPs peaked at different wavelengths for near-room-temperature operation. At 250 K, ideal performance can be reached for typical QWIPs up to a detection wavelength of 12 μm , under a laser power density of 0.1 $\text{mW}/\mu\text{m}^2$. To validate the predictions, we measured the dark currents of QWIP samples at high operating temperatures. Theoretical results are in good agreement with the experimental data.

¹ Key Laboratory of Artificial Structures and Quantum Control (Ministry of Education), Department of Physics and Astronomy, Shanghai Jiao Tong University, Shanghai 200240, China

² Institute of Ion-Beam Physics and Materials Research, Helmholtz-Zentrum Dresden-Rossendorf 01314, Dresden, Germany

*Corresponding authors: e-mail: mrhao@sjtu.edu.cn; wzshen@sjtu.edu.cn; h.schneider@hzdr.de

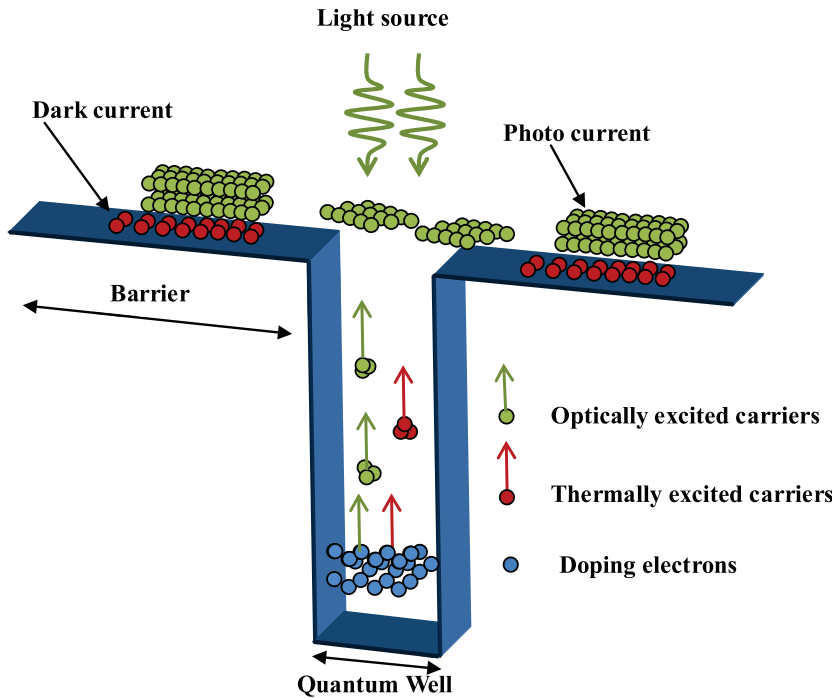


Figure 1 The schematic shows the photon-noise-limited performance of the QWIP. Under laser light illumination, the current flowing above the barrier is dominated by the photocurrent.

2. Discussion

QWIP noise is caused by carrier density fluctuations originating from random thermal and photon excitation. According to the origins, it is normally categorized into three types, device noise from dark current, background noise from background radiation, and signal noise from incident signal light. Signal noise is typically much smaller than the other two for usual applications such as infrared thermal imaging. To achieve high performance, infrared photodetectors are typically cryogenically cooled to suppress thermal generation and thus dark current noise. When the operating temperature is low enough, background noise dominates over the device noise, and background-limited performance is achieved.

However, the signal photocurrent can become much larger than the dark current and the background photocurrent when the photodetector is illuminated by a strong infrared laser source (e.g., a QCL or a CO₂ laser), and the signal noise becomes the major noise source. In such a case, the performance of the device is determined by the signal radiation and we call this photon-noise-limited performance (PLIP). Under this condition, the signal-to-noise ratio of the detector is optimum in the sense that it cannot be improved any more by reducing the operating temperature. Figure 1 shows the principal processes of the PLIP regime in a QW structure. Within this model for QWIPs, the total current I_{tot} is composed of three parts, dark current I_{dark} generated from thermal activation, background current I_{B} from background radiation in the detector field of view, and signal current I_{S} from signal photon flux. The total current can therefore be expressed as

$$I_{\text{tot}} = I_{\text{dark}} + RP_{\text{B}} + RP_{\text{S}}. \quad (1)$$

Here, R is the detector responsivity. P_{B} and P_{S} are the incident powers of background radiation and signal, respectively.

We consider a typical QWIP with a bound-to-quasibound intersubband transition scheme. Here, electrons are photoexcited from a confined state with energy E_1 , into an excited state E_2 , which is in resonance with the barrier V_{b} ($E_2 \approx V_{\text{b}}$). The barriers are assumed to be sufficiently thick and the number of quantum well (QW) repeats sufficiently large to allow us to neglect interwell tunneling and contact effects. All carriers in the QW structure originate from doping assuming complete ionization. Electrons distribute according to Fermi–Dirac statistics involving a two-dimensional (2D) density of states $\rho_{2\text{D}}$ in the well and an unbound three-dimensional (3D) density of states $\rho_{3\text{D}}$ above the barrier. Thus, the Fermi level dependence of the sheet doping level and temperature is determined by

$$N_{\text{d}} = \int_0^{\infty} \rho_{2\text{D}}(\varepsilon) f(\varepsilon) \text{d}\varepsilon + L_{\text{p}} \int_{V_{\text{b}}-E_1}^{\infty} \rho_{3\text{D}}(\varepsilon) f(\varepsilon) \text{d}\varepsilon, \quad (2)$$

where N_{d} is the sheet doping density in each quantum well, L_{p} is the quantum well period (sum of well width L_{w} and barrier width L_{b}). The energy distribution $f(\varepsilon)$ is given by the Fermi–Dirac distribution $f(\varepsilon) = 1 / (1 + \exp(\frac{\varepsilon - E_{\text{F}}}{k_{\text{B}}T}))$, where E_{F} is the Fermi level referenced to the ground-state energy E_1 , k_{B} is the Boltzmann constant and T is the temperature.

For QWIPs operated close to room temperature, only a small bias voltage is required. Thermionic emission current is the major dark current component, neglecting resonant, interwell and thermally assisted tunnelings. The dark current density J_{dark} is estimated using the 3D carrier drift

model [1] by accounting for the carriers thermally excited out of the well and flowing above the barriers. Therefore, J_{dark} is given by

$$J_{\text{dark}} = eN_{3\text{D}}V_{\text{drift}}(F), \quad (3)$$

where e is electron charge and $V_{\text{drift}}(F)$ is the average drift velocity in the barrier as a function of electric field F . Neglecting diffusion processes, the average drift velocity takes the usual form $V_{\text{drift}}(F) = \mu F / [1 + (\mu F / v_{\text{sat}})^2]^{1/2}$, where μ is the low-field mobility and v_{sat} is the saturated drift velocity. The 3D mobile electron density on top of the barriers $N_{3\text{D}}$ is calculated by

$$N_{3\text{D}} = 2 \left(\frac{m_b^* k_B T}{2\pi \hbar^2} \right)^{3/2} \exp\left(-\frac{E_{\text{act}}}{k_B T}\right), \quad (4)$$

where \hbar is the reduced Planck constant, m_b^* is the barrier effective mass, E_{act} is the thermal activation energy that equals the energy difference between the barrier height and the Fermi level in the well. Neglecting the bias-field-induced barrier lowering effect, we have $E_{\text{act}} = V_b - E_F$.

The signal current density J_{photo} is given by the standard expression

$$J_{\text{photo}} = e\eta g \Phi_s, \quad (5)$$

where η is the absorption quantum efficiency, Φ_s is photon number flux density of the signal, g is photoconductive gain that equals the ratio of the photoelectron capture lifetime to the transit time across the device. The transit time can be estimated by $\tau_{\text{trans}} \approx NL_p / V_{\text{drift}}(F)$. The photoconductive gain is then given by

$$g = \frac{\tau_{\text{cap}} V_{\text{drift}}(F)}{NL_p}, \quad (6)$$

where τ_{cap} is the electron capture time into the well, and N is the number of QWs.

The electron capture time at liquid-nitrogen temperature is determined by the LO phonon scattering and an expression has been given in Ref. [17],

$$\tau_{\text{cap}} = \frac{4h\varepsilon_p E_c L_p}{e^2 E_{\text{phonon}} I_1}, \quad (7)$$

where E_c is the cutoff energy, E_{phonon} is the optical phonon energy, $\varepsilon_p^{-1} = \varepsilon(\infty)^{-1} - \varepsilon(0)^{-1}$, $\varepsilon(0)$ and $\varepsilon(\infty)$ is the static and high-frequency dielectric permittivity, respectively. I_1 is a dimensionless integral whose value is close to 2 in the 3–19 μm cutoff wavelength range. The temperature dependence of the LO phonon scattering rate is predicted by the phonon occupation number factor. In the range close to room temperature, a good approximation for the capture time is

$$\tau_{\text{cap}}(T)^{-1} = \tau_{\text{cap}}^{-1} \left[1 + \frac{2}{\exp(E_{\text{phonon}}/k_B T) - 1} \right]. \quad (8)$$

$1/f$ noise, is observed in the low-frequency range for most detector technologies, but it is especially weak for QWIPs and does not play any role in practical systems. Therefore, we neglected the influence of $1/f$ noise here. The generation–recombination noise is described as $i_{\text{noise,dark}}^2 = 4egJ_{\text{dark}}A\Delta f$, where Δf is the measurement bandwidth and A is detector area. The noise-equivalent power (NEP) is the signal power needed to produce the same signal strength as produced by a noise source. According to the above analysis, the dark current noise-limited (NEP)_{dark} is

$$(\text{NEP})_{\text{dark}} = \frac{2hc}{\lambda_s \eta^{(1)}(T)} \sqrt{\frac{N_{3\text{D}} L_p}{\tau_{\text{cap}}(T) N}} \sqrt{A \Delta f}, \quad (9)$$

where λ_s is the signal wavelength and $\eta^{(1)}(T)$ is the temperature-dependent peak absorption quantum efficiency for one well. The dark current noise-limited detectivity is

$$D_{\text{dark}}^* = \frac{\lambda_s \eta^{(1)}(T)}{2hc} \sqrt{\frac{\tau_{\text{cap}}(T) N}{N_{3\text{D}} L_p}}. \quad (10)$$

Close to room temperature, PLIP operation requires that J_{photo} is larger than J_{dark} , such that the minimum signal power P_{PLIP} is given by

$$P_{\text{PLIP}} = \frac{hc}{\lambda_s} \frac{N_{3\text{D}}}{\tau_{\text{cap}}(T)} \frac{L_p}{\eta^{(1)}(T)} A, \quad (11)$$

For PLIP operation, the total noise is $i_{\text{noise}}^2 = i_{\text{noise,dark}}^2 + i_{\text{noise,photon}}^2$, where the photocurrent noise $i_{\text{noise,photon}}^2 = 4egJ_{\text{photo}}A\Delta f$. Assuming $J_{\text{photo}} = nJ_{\text{dark}}$, $n \geq 1$, the near-PLIP detectivity is given by

$$D_{\text{near-PLIP}}^* = \frac{\lambda_s \eta^{(1)}(T)}{2\sqrt{1+n^2} hc} \sqrt{\frac{\tau_{\text{cap}}(T) N}{N_{3\text{D}} L_p}}. \quad (12)$$

If the photocurrent is much larger than the dark current, the total noise is dominated by the photon noise so that the square noise level is $(4eg\Delta f)$ times the signal power. So, the $\text{NEP}_{\text{PLIP}} = 4hc\Delta f/\lambda_s \eta$ as a figure of merit is not applicable. Therefore, SNR is preferred to describe the detector performance and is given by

$$\begin{aligned} \frac{S}{N} &= \frac{J_{\text{photo}} A}{\sqrt{A \Delta f (4egJ_{\text{dark}} + 4egJ_{\text{photo}})}} \\ &= \sqrt{\frac{n}{n+1}} \sqrt{\frac{\eta(T) \phi_s A}{4\Delta f}}. \end{aligned} \quad (13)$$

If the signal power satisfies Eq. (11), i.e. $J_{\text{photo}} = J_{\text{dark}}$, the corresponding SNR is $\sqrt{\eta(T) \phi_s A / 8\Delta f}$. If $J_{\text{photo}} \gg J_{\text{dark}}$, the SNR is $\sqrt{\eta(T) \phi_s A / 4\Delta f}$. For the ideal case $\eta(T) = 1$, the SNR is limited to a value of $\sqrt{\phi_s A / 4\Delta f}$, which is determined by the signal flux density, detector area and the measurement bandwidth.

The temperature-dependent absorption of a single QW is proportional to the occupation density of the ground state,

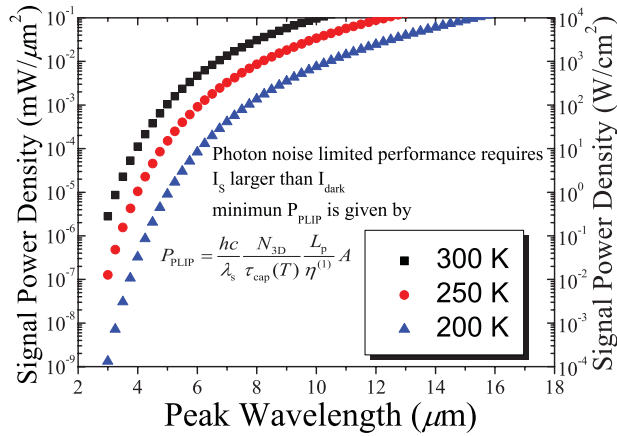


Figure 2 Calculated minimum signal power density for QWIPs with different peak wavelengths achieve photon-noise limited performance at 200, 250 and 300 K.

taking into account the impact of the spectral broadening [18]

$$\eta^{(1)}(T) = \frac{\kappa}{\delta E} \frac{m_b^* k_B T}{\pi \hbar^2} \ln \left[\exp \left(\frac{E_F}{k_B T} \right) + 1 \right], \quad (14)$$

where κ represents the proportionality coefficient that is related to the QW structure parameters, δE is the half-width at half-maximum of the absorption lineshape. Combining Eq. (14) with Eqs. (4) and (11), the doping-density-dependent minimum signal power P_{PLIP} is a function of $E_F/k_B T$ and proportional to

$$P_{\text{PLIP}} \propto \frac{\exp \left(\frac{E_F}{k_B T} \right)}{\ln \left[\exp \left(\frac{E_F}{k_B T} \right) + 1 \right]}. \quad (15)$$

This expression shows that the way of obtaining low PLIP signal power is to reduce $E_F/k_B T$. However, low doping will also degrade the absorption and signal-to-noise ratio. If we replace the signal radiation by background radiation, the derivation of the minimum P_{PLIP} is essentially equivalent to the maximum ratio of photocurrent to dark current, which is similar to the discussion on the maximum BLIP temperature in Ref. [19]. The optimal doping was not predicted from our calculation if the photons are efficiently absorbed. Therefore, we face a trade-off between the PLIP signal power and signal-to-noise ratio. The doping density should be low enough to get a moderate PLIP signal power, but high enough to get a good signal-to-noise ratio.

Following Refs. [1] and [20], we take the room-temperature absorption per quantum well per pass to be about 0.54% for polarized light for a 2D electron density of $5 \times 10^{11} \text{ cm}^{-2}$. Considering typical QWIP designs with different peak response wavelengths, the minimum signal power for near-room-temperature operation is obtained from Eq. (11). Figure 2 shows the calculated signal power densities for detection peak wavelength in the 3–16 μm band.

In practice, and according to our previous experiments, QWIPs can easily withstand a cw laser power of 10 mW [20]. The smallest device in our past experiments had an area of $10 \mu\text{m} \times 10 \mu\text{m}$ (for ultrahigh-speed operation) [20]. However, in practice the detector size does not need to be that small for other wavelengths. As long as the signal radiation power density reaches the threshold value, the PLIP condition will be satisfied. Using a high-power quantum cascade laser (QCL) as the source, in a limiting case of having 10 mW power coupled to a $10 \mu\text{m} \times 10 \mu\text{m}$ -area QWIP, the signal power density is $0.1 \text{ mW}/\mu\text{m}^2$. A sensing system as described here works in pulsed mode or with infrared signals modulated at relatively high frequencies, for which the bolometric response can be neglected [15].

Figure 2 therefore predicts that up to a peak wavelength of 10 μm QWIPs can work at signal-limited performance at 300 K, which is consistent with our previous experiments [20]. At 250 K, a temperature easily reachable with a thermoelectric Peltier cooler (TEC), this ideal performance can be achieved for QWIPs below 12 μm peak wavelength. At 200 K, the lowest temperature a TEC can reach, QWIPs can operate in the PLIP regime for the whole 3–15 μm peak wavelength band. From our calculation the minimum signal power density decreases rapidly when the detection wavelength becomes shorter, since an increase in activation energy exponentially decreases the dark current. At 250 K, the signal power density to achieve PLIP is two orders of magnitude larger for QWIPs with 10 μm detection wavelength than for QWIPs operating at 5 μm . PLIP is much easier to achieve for peak wavelengths in the 3–5 μm range than in the 8–14 μm range.

QWIPs have advantages in their wide dynamic range and stability, as compared to other types of mid-infrared photodetectors [21]. The saturation signal intensity is estimated to be over $300 \text{ kW}/\text{cm}^2$ [22], and nonlinearity can be decreased or completely suppressed in QWIPs with a large number of QWs [23].

3. Experimental

We use the 3D carrier drift model to estimate the dark-current level in QWIPs, assuming that thermionic emission is the major dark-current contribution. In the calculation, the Fermi level is a function of both temperature and doping density instead of simply being proportional to the 2D doping density of the well. To validate our analysis, we have measured the dark currents of a series of QWIPs at different temperatures ranging from 150 K to room temperature, and compared the results with model calculations.

The QWIPs under study were fabricated by molecular beam epitaxy on semi-insulating GaAs substrates. All QWIPs have the same structural parameters except for the Si doping densities in the quantum wells. The QWIPs with bound-to-quasibound design are peaked at a wavelength of 9 μm . The QWIPs consist of 100 periods of 54 \AA thick GaAs

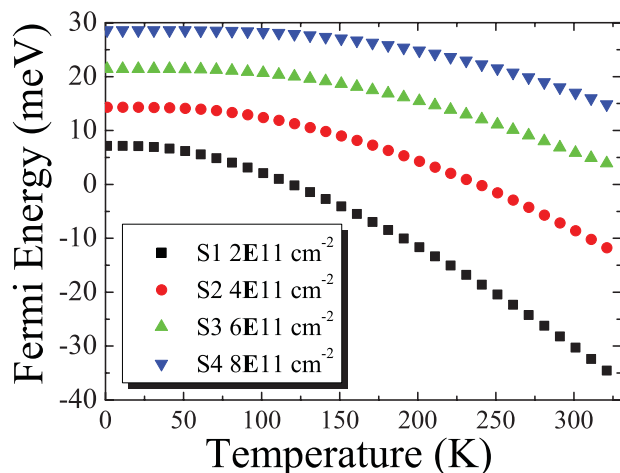


Figure 3 Calculated Fermi energy versus temperature for various QWIP samples. The sample structure parameters were selected for a peak absorption wavelength near $9\ \mu\text{m}$. The 2D doping densities are 2×10^{11} , 4×10^{11} , 6×10^{11} and $8 \times 10^{11}\ \text{cm}^{-2}$ for samples S1, S2, S3 and S4, respectively. The Fermi energy value is referenced to the ground-state energy in the well.

wells and $300\ \text{\AA}$ thick $\text{Al}_{0.24}\text{Ga}_{0.76}\text{As}$ barriers sandwiched between an 8000-\AA thick GaAs bottom contact and a 4000-\AA thick GaAs top contact, Samples S1, S2, S3, and S4 were delta doped in the GaAs well with Si to 2D concentrations of 2×10^{11} , 4×10^{11} , 6×10^{11} and $8 \times 10^{11}\ \text{cm}^{-2}$, respectively. The experiments were performed on $240\ \mu\text{m} \times 240\ \mu\text{m}$ mesas formed by standard photolithography with wet chemical etching and ohmic contact metallization. Temperature-dependent dark-current measurements were carried out in a closed-cycle refrigerator using a Keithley 2400 source meter. More details about other measurements can be found in Ref. [24].

Here, we analyze the temperature dependence of the dark currents for samples with different doping densities to validate our dark-current model close to room temperature. The number of electrons above the barriers is determined by thermally generated carriers and depends exponentially on the distance above the Fermi energy. According to Eq. (2) we numerically calculate the Fermi energy for our samples with different 2D doping densities. Figure 3 shows the temperature dependence of the Fermi energy for Samples S1, S2, S3 and S4. It is seen that the Fermi energy remains nearly unchanged at low temperature ($<77\ \text{K}$) and decreases significantly with increasing temperature up to room temperature. We take the 3D carrier drift model to calculate thermionic emission processes that dominate the dark current. Equations (3) and (4) give the theoretical predictions of the dark current for our samples. Figure 4 shows representative dark-current measurement results and simulations of Sample S2 at different temperatures. It is evident that experimental data (dots) are in good agreement with the model results (lines) from 150 to 300 K. The good agreement is seen for all four samples, thus indicating that our dark current model is valid for QWIPs in this temperature

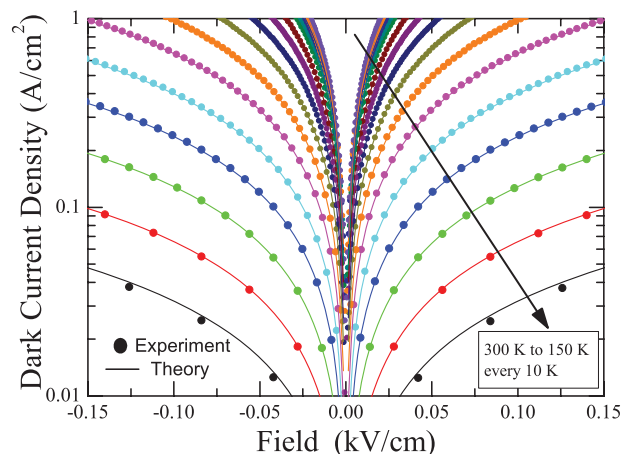


Figure 4 Dark current density versus bias voltage of sample S2 from 150 to 300 K. Experimental data are shown as dots and theoretical values are shown as lines.

region. Both the photocurrent and the photon noise current are proportional to the photoconductive gain. Since the gain cancels out in the expression for SNR, the responsivity will not change too much the PLIP condition. Therefore, using the 3D carrier drift model based on thermal excitation, we can reliably determine the laser power requirement to reach PLIP for QWIPs.

4. Conclusion

We have presented a theoretical and experimental analysis to investigate the laser power requirement for achieving the photon-noise-limited performance of QWIPs with different peak response wavelengths close to room temperature. Comparing these calculations with experimental dark current data, we demonstrate that the model is valid in this temperature region. Based on our analysis, this ideal performance can be reached for QWIPs with peak wavelength below $12\ \mu\text{m}$ up to 250 K, which is easily reachable with a thermoelectric Peltier cooler. Therefore, QWIPs are suited for compact detection systems operating up to or near room temperature.

Acknowledgements. This work was supported in part by the National Major Basic Research Projects (2011CB925603), Natural Science Foundation of China (91221201, 61234005 and 11074167), China Post Doctoral Science Foundation General Financial Grant (2012M520890) and the 863 Program (2011AA010205).

Received: 9 September 2013, **Revised:** 30 November 2013, **Accepted:** 17 December 2013

Published online: 16 January 2014

Key words: Quantum well infrared photodetector, QWIP, photon-noise-limited performance, background-limited performance.

References

- [1] H. Schneider and H. C. Liu, *Quantum Well Infrared Photodetectors-Physics and Applications* (Springer, New York, 2007) Chap. 4.
- [2] S. D. Gunapala, S. V. Bandara, J. K. Liu, J. M. Mumolo, D. Z. Ting, C. J. Hill, J. Nguyen, B. Simolon, J. Woolaway, and S. C. Wang, *IEEE J. Quantum Electron.* **46**, 285–293 (2010).
- [3] K. K. Choi, D. P. Forrai, D. W. Endres, and J. Sun, *IEEE J. Quantum Electron.* **45**, 1255–1264 (2009).
- [4] R. Paiella, R. Martini, F. Capasso, C. Gmachl, H. Y. Hwang, D. L. Sivco, J. N. Baillargeon, A. Y. Cho, E. A. Whittaker, and H. C. Liu, *Appl. Phys. Lett.* **79**, 2526–2528 (2001).
- [5] A. Hugi, G. Villares, S. Blaser, H. C. Liu, and J. Faist, *Nature* **492**, 229–233 (2012).
- [6] F. K. Tittel, Y. Bakhirkin, A. A. Kosterev, and G. Wysocki, *Rev. Laser Eng.* **34**, 275–282 (2006).
- [7] A. Kosterev, G. Wysocki, Y. Bakhirkin, S. So, R. Lewicki, M. Fraser, F. K. Tittel, and R. Curl, *Appl. Phys. B.* **90**, 165–176 (2008).
- [8] H. Schneider, C. Schönbein, M. Walther, K. Schwarz, J. Fleissner, and P. Koidl, *Appl. Phys. Lett.* **71**, 246–248 (1997).
- [9] L. Gendron, M. Carras, A. Huynh, V. Ortiz, C. Koeniguer, and V. Berger, *Appl. Phys. Lett.* **85**, 2824–2826 (2004).
- [10] A. Shen, H. C. Liu, M. Gao, E. Dupont, M. Buchanan, J. Ehret, G. J. Brown, and F. Szmulowicz, *Appl. Phys. Lett.* **77**, 2400–2402 (2000).
- [11] T. Töpfer, K. P. Petrov, Y. Mine, D. Jundt, R. F. Curl, and F. K. Tittel, *Appl. Opt.* **36**, 8042–8049 (1997).
- [12] F. K. Tittel, G. Wysocki, A. Kosterev, and Y. Bakhirkin, *Mid-infrared Coherent Sources and Applications*, (Springer, Dordrecht, 2008), p. 467.
- [13] A. Bauer, K. Rößner, T. Lehnhardt, M. Kamp, S. Höfling, L. Worschech, and A. Forchel, *Semicond. Sci. Technol.* **26**, 014032–014040 (2010).
- [14] H. C. Liu, J. Li, E. R. Brown, K. McIntosh, K. B. Nichols, and M. Manfra, *Appl. Phys. Lett.* **67**, 1594–1596 (1995).
- [15] P. Grant, R. Dudek, M. Buchanan, and H. C. Liu, *IEEE Photon. Technol. Lett.* **18**, 2218–2220 (2006).
- [16] F. Capasso, *Opt. Eng.* **49**, 111102–111102 (2010).
- [17] J. Y. Andersson, *J. Appl. Phys.* **78**, 6298–6304 (1995).
- [18] H. C. Liu, *J. Appl. Phys.* **73**, 3062–3067 (1993).
- [19] M. R. Hao, S. Zhang, Y. H. Zhang, W. Z. Shen, H. Schneider, and H. C. Liu, *IEEE J. Quantum Electron.* **50**, 3–6, (2014).
- [20] H. C. Liu, R. Dudek, A. Shen, E. Dupont, C. Song, Z. R. Wasilewski, and M. Buchanan, *Appl. Phys. Lett.* **79**, 4237–4239 (2001).
- [21] S. D. Gunapala, S. V. Bandara, J. K. Liu, S. B. Rafol, J. M. Mumolo, C. A. Shott, R. Jones, J. Woolaway, J. M. Fastenau, and A. K. Liu, *Infrared. Phys. Technol.* **44**, 411–425 (2003).
- [22] F. H. Julien, J. M. Lourtioz, N. Herschkorn, D. Delacourt, J. P. Pocholle, M. Papuchon, R. Planel, and G. Le Roux, *Appl. Phys. Lett.* **53**, 116–118 (1988).
- [23] M. Ershov, H. C. Liu, M. Buchanan, Z. Wasilewski, and V. Ryzhii, *Appl. Phys. Lett.* **70**, 414–416 (1997).
- [24] Y. Yang, H. C. Liu, W. Z. Shen, N. Li, W. Lu, Z. R. Wasilewski, and M. Buchanan, *IEEE J. Quantum Electron.* **45**, 623–628 (2009).